Journal of Sound and Vibration (1999) **221**(3), 443–470
Article No. jsvi.1998.2034, available online at http://www.idealibrary.com on IDEAL

FREE VIBRATION OF LAMINATED COMPOSITE PLATES WITH CUTOUT

K. SIVAKUMAR, N. G. R. IYENGAR
Department of Aerospace Engineering, *Indian Institute of Technology*, *Kanpur* 208016, *India*

AND

K. DEB
Department of Mechanical Engineering, *Indian Institute of Technology*, *Kanpur* 208016, *India*

(*Received* 16 *April* 1998, *and in final form* 30 *September* 1998)

The present investigation is concerned with free vibration analysis of composite plates in the presence of cutouts undergoing large amplitude oscillations. The Ritz finite element model using a nine-noded C^0 continuity, isoparametric quadrilateral element along with a higher order displacement theory which accounts for parabolic variation of transverse shear stresses is used to predict the dynamic behavior. Results have been obtained for laminated plates with various cutout geometries such as square, rectangle, circle and ellipse in the large amplitude range. Backbone curves are drawn for various boundary conditions and aspect ratios of the cutout.

1. INTRODUCTION

Cutouts are inevitable in structures. Cutouts in structural members like aircraft wings made up of composite laminates may result in a change in the dynamic characteristics. Its effects are likely to be quite considerable when the plate is undergoing large oscillations, specifically in space craft or aircraft structures where thin skins are used. The undesirable vibrations may cause sudden failures due to resonance in the presence of cutouts. It is, therefore, important to predict the natural frequencies of these structural members accurately. Woinowsky-Krieger [1] were probably the first to provide an exact solution using the elliptic integral method for the non-linear vibration of simply supported uniform isotropic beams with immovable ends. These isotropic plates undergoing large amplitude vibrations have been investigated by using the continuum approach by Wah [2], Chu and Herrman [3], Yamaki [4] and Aalami [5], and the finite element method by Mei [6] and Rao *et al*. [7]. Chandra and Basavaraju [8, 9] discuss the large deflection vibration of cross ply and angle ply laminated plates using the perturbation technique. The dynamic analogies of Von-Karman's large deflection equations for laminated plates are used. Raju *et al*. [10] studied the

0022–460X/99/130443 + 28 $30.00/0

effects of longitudinal or in-plane deformation and inertia on large amplitude flexural vibrations of slender beams and thin plates. Kanaka Raju and Hinton [11] studied the large amplitude vibrations of Mindlin plates using Lagrangian isoparametric quadrilateral elements with selective integration. Reddy and Chao [12] presented a finite element analysis of the large-deflection theory (in Von-Karman's sense) including transverse shear, for moderately thick laminated anisotropic composite plates. Linear quadratic rectangular elements with five degrees of freedom per node are employed to analyse rectangular plates subjected to various loadings and edge conditions. Reddy [13] studied the effect of square cutout on the behavior of the laminated plate undergoing large amplitude vibration. He considered two-layer angle ply and cross ply laminates for this study. Putcha and Reddy [14] developed a refined mixed shear finite element for the non-linear bending analysis of laminated plates. Non-linear bending analysis of a laminated plate with a higher-order theory and with a higher-order C^1 continuous refined finite element method for laminated beams and plates were given by Gajbir *et al.* [15–17]. Non-linear forced and free vibration analysis of laminated composite plates with a higher-order theory and with a higher-order C^1 continuous refined finite element were reported by Gajbir *et al.* [18–20]. Chandrasekhara and Tenneti [21] carried out the non-linear static and dynamic analyses of heated laminated plates using a shear flexible finite element approach. Their model accounts for large deflections of the plate and non-uniform distributions of temperature. A nine-noded isoparametric element is used to obtain the numerical solutions. Bharat *et al.* [22] discussed an analytical solution for the large amplitude free-vibration of antisymmetric cross ply rectangular composite plates having an additional quadratic non-linear term in the model equation of equilibrium.

It is shown that the classical two-term perturbation solution and further extension of the same for a five-term solution fail to yield any meaningful results when the coefficients of non-linear terms in the modal equations are large. Hence, an iteration method used to solve the Duffing's equation for isotropic plates is extended to solve the present problem. Shi and Mei [23, 24] developed a time domain formulation for the large amplitude free vibration of plates. The procedure of deriving the non-linear equations of motion are discussed and accurate frequency–maximum deflection relations are obtained for the fundamental and higher non-linear modes. Very few attempts have been made to predict the large amplitude behavior of laminated plates in the presence of cutouts. In the present work, a detailed study has been carried out on large amplitude oscillations of the laminated plates in the presence of various types of centrally placed cutouts.

2. FORMULATION FOR LARGE AMPLITUDE VIBRATION

The problem is formulated for a plate of thickness h composed of orthotropic layers of thickness h_i with fibers oriented at angles $\pm\theta$, as shown in Figure 1.

The higher-order displacement model which gives parabolic variation of shear stresses across the thickness of the laminate, is given as [25]

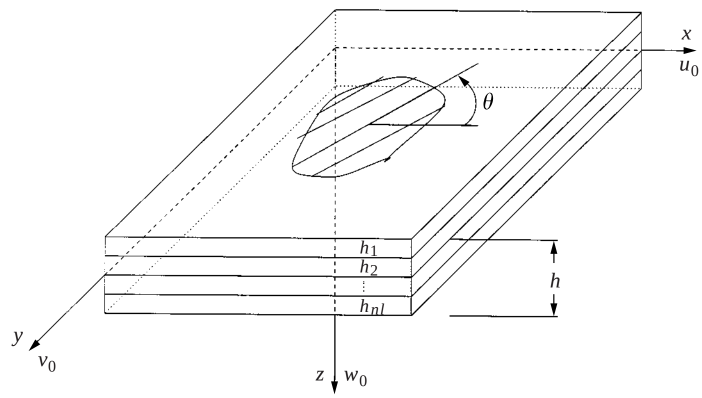

Figure 1. Laminated plate with co-ordinates and displacements.

$$\begin{aligned} u(x, y, z, t) &= u_0(x, y, t) + f_1(z)\psi_x(x, y, t) + f_2(z)\theta_x(x, y, t), \\ v(x, y, z, t) &= v_0(x, y, t) + f_1(z)\psi_y(x, y, t) + f_2(z)\theta_y(x, y, t), \\ w(x, y, z, t) &= w_0(x, y, t), \end{aligned} \tag{1}$$

where

$$f_1(z) = C_1 z - C_2 z^3, \qquad f_2(z) = -C_4 z^3, \tag{2, 3}$$

with $C_1 = 1$, and $C_2 = C_4 = 4/3h^2$. u, v and w are the displacements along the x, y and z directions. u_0, v_0 and w_0 are displacements of the middle plane of the laminate and θ_x, θ_y, ψ_x and ψ_y are the rotations and slope respectively along the x and y axes.

From the Green's strain vector, the non-linear strain displacement relation is given in reference [26] as

$$\left\{ \begin{array}{c} \varepsilon_x \\ \varepsilon_y \\ \gamma_{xy} \\ \gamma_{xz} \\ \gamma_{yz} \end{array} \right\} = \left\{ \begin{array}{c} u_{,x} + \frac{1}{2}(u_{,x}^2 + \frac{1}{2}v_{,x}^2 + \frac{1}{2}w_{,x}^2) \\ v_{,y} + \frac{1}{2}(u_{,y}^2 + \frac{1}{2}v_{,y}^2 + \frac{1}{2}w_{,y}^2) \\ u_{,y} + v_{,x} + u_{,x}u_{,y} + v_{,x}v_{,y} + w_{,x}w_{,y} \\ u_{,z} + w_{,x} + u_{,x}u_{,z} + v_{,x}v_{,z} + w_{,x}w_{,z} \\ v_{,z} + w_{,y} + u_{,z}u_{,y} + v_{,z}v_{,y} + w_{,z}w_{,y} \end{array} \right\}, \tag{4}$$

where

$$\{\varepsilon\} = \{\varepsilon\}^L + \{\varepsilon\}^{NL}, \tag{5}$$

in which the strain displacement relations corresponding to the model mentioned above are

$$\{\varepsilon\}^L = \begin{Bmatrix} \varepsilon_p^L \\ 0 \end{Bmatrix} + \begin{Bmatrix} z\varepsilon_b^L \\ \varepsilon_s \end{Bmatrix} + \begin{Bmatrix} 0 \\ z^2\varepsilon_s^* \end{Bmatrix} + \begin{Bmatrix} z^3\varepsilon^* \\ 0 \end{Bmatrix},$$

$$\{\varepsilon_p^L\} = \begin{Bmatrix} u_{0,x} \\ v_{0,y} \\ u_{0,y} + v_{0,x} \end{Bmatrix}, \quad \{\varepsilon_b^L\} = C_1 \begin{Bmatrix} \psi_{x,x} \\ \psi_{y,y} \\ \psi_{x,y} + \psi_{y,x} \end{Bmatrix},$$

$$\{\varepsilon^*\} = -C_2 \begin{Bmatrix} \psi_{x,x} \\ \psi_{y,y} \\ \psi_{x,y} + \psi_{y,x} \end{Bmatrix} - C_4 \begin{Bmatrix} \theta_{x,x} \\ \theta_{y,y} \\ \theta_{x,y} + \theta_{y,x} \end{Bmatrix},$$

$$\{\varepsilon_s\} = C_1 \begin{Bmatrix} \psi_y \\ \psi_x \end{Bmatrix} + \begin{Bmatrix} w_{0,y} \\ w_{0,x} \end{Bmatrix}, \quad \{\varepsilon_s^*\} = -3C_2 \begin{Bmatrix} \psi_y \\ \psi_x \end{Bmatrix} - 3C_4 \begin{Bmatrix} w_{0,y} \\ w_{0,x} \end{Bmatrix}.$$

Assuming that the plate is moderately thick and strains are much smaller than the rotations, one can rewrite non-linear components of equation (4) as

$$\{\varepsilon^{NL}\} = \begin{Bmatrix} \frac{1}{2} w_{,x}^2 \\ \frac{1}{2} w_{,y}^2 \\ w_{,x} w_{,y} \\ 0 \\ 0 \end{Bmatrix}. \tag{6}$$

This corresponds to the well known Von-Karman's relationships for large displacements.

The stress–strain relations for the kth lamina oriented at an arbitrary angle, θ, with respect to the reference axis are

$$\begin{Bmatrix} \sigma_x \\ \sigma_y \\ \tau_{xy} \\ \tau_{xz} \\ \tau_{yz} \end{Bmatrix}_k = \begin{bmatrix} \bar{Q}_{11} & \bar{Q}_{12} & \bar{Q}_{16} & 0 & 0 \\ \bar{Q}_{21} & \bar{Q}_{22} & \bar{Q}_{26} & 0 & 0 \\ \bar{Q}_{16} & \bar{Q}_{26} & \bar{Q}_{66} & 0 & 0 \\ 0 & 0 & 0 & \bar{Q}_{44} & \bar{Q}_{45} \\ 0 & 0 & 0 & \bar{Q}_{54} & \bar{Q}_{55} \end{bmatrix}_k \begin{Bmatrix} \varepsilon_x \\ \varepsilon_y \\ \gamma_{xy} \\ \gamma_{xz} \\ \gamma_{yz} \end{Bmatrix}_k, \tag{7}$$

or

$$\{\sigma_i\} = [\bar{Q}_{ij}]\{\varepsilon_j\}, \tag{8}$$

where $\bar{Q}_{ij}$'s are the transformed stiffness coefficients.

2.1. ENERGY EQUATIONS

The strain energy of the plate is given by

$$U = \frac{1}{2}\int_v \varepsilon_i^T \sigma_i \, \mathrm{d}V. \tag{9}$$

The five strain components (plane stress condition) may be represented as ε_i and stress components as σ_i and for linear elastic constitutive matrix C_{ij} ($C_{ij} = \bar{Q}_{ij}$), the constitutive relations are given by

$$\sigma_i = C_{ij}\varepsilon_j, \tag{10}$$

The strain energy U can then be written as

$$\begin{aligned} U &= \frac{1}{2}\int\int\int \{\varepsilon\}^T C_{ij}\{\varepsilon\}\, \mathrm{d}x\, \mathrm{d}y\, \mathrm{d}z \\ &= \frac{1}{2}\int\int\int \{\varepsilon^L + \varepsilon^{NL}\}^T C_{ij}\{\varepsilon^L + \varepsilon^{NL}\}\, \mathrm{d}x\, \mathrm{d}y\, \mathrm{d}z \\ &= \frac{1}{2}\int\int\int \{C_{ij}(\varepsilon^L\varepsilon^L + 2\varepsilon^L\varepsilon^{NL} + \varepsilon^{NL}\varepsilon^{NL})\}\, \mathrm{d}x\, \mathrm{d}y\, \mathrm{d}z. \end{aligned} \tag{11}$$

The strain component ε_i can be expressed as

$$\varepsilon_i = L_i^T d + \frac{1}{2} d^t H_i d, \tag{12}$$

in which L_i is a vector, H_i is a symmetric matrix and d is the vector of displacement gradients contributing to the strains. Using the procedure adopted by Rajasekaran and Murrary [27] for isotropic plates and Ganapathi and Varadan [28] for composite laminates, the strain energy expression (membrane and bending) with higher order shear deformation theory for large amplitude free vibration can be written as

$$U_{MB} = \frac{1}{2}\int\int d^T\left[\frac{1}{2}[NA] + \frac{1}{6}[NB] + \frac{1}{12}[NC]\right] d\, \mathrm{d}x\, \mathrm{d}y. \tag{13}$$

Derivative of the displacements which contribute to the strain can be expressed in vector form as

$$d^T = \langle u_{,x}\ u_{,y}\ v_{,x}\ v_{,y}\ w_{,x}\ w_{,y}\ \psi_{x,x}\ \psi_{y,y}\ (\psi_{y,x}, \psi_{x,y})\ \theta_{x,x}\ \theta_{y,y}\ (\theta_{y,x}, \theta_{x,y})\rangle$$

The components of linear ($[NA]$) and non-linear stiffness matrices ($[NB]$, $[NC]$) are given in Appendix A.

Strain energy due to shear is expressed as,

$$U_S = \frac{1}{2}\int\int d_s^T [NS] d_s\, \mathrm{d}x\, \mathrm{d}y, \tag{14}$$

where

$$[NS] = \begin{bmatrix} [A_1] & [D_1] \\ [D_1] & [F_1] \end{bmatrix}, \tag{15}$$

and

$$(A_{1_{ij}}, D_{1_{ij}}, F_{1_{ij}}) = \int_{-h/2}^{h/2} \bar{Q}_{ij}(1, z^2, z^4)\, \mathrm{d}z \text{ for } i, j = 4, 5.$$

The total strain energy for the laminate is therefore

$$U = U_{MB} + U_S. \tag{16}$$

The kinetic energy of the laminate can be expressed in terms of nodal degrees of freedom as

$$T = \frac{1}{2}\int_A \left(\sum_{k=1}^{nl} \int_{z_{k-1}}^{z_k} \rho^{(k)} \dot{\bar{u}}^T \dot{\bar{u}} \, \mathrm{d}z \right) \mathrm{d}A. \tag{17}$$

Here $\bar{u}$ is the global displacement vector and is given by

$$\{\bar{u}\} = \{u \; v \; w\}^T, \tag{18}$$

with

$$\{\bar{u}\} = [\bar{N}]\{\delta\}, \tag{19}$$

where

$$[\bar{N}] = \begin{bmatrix} 1 & 0 & 0 & f_1(z) & 0 & f_2(z) & 0 \\ 0 & 1 & 0 & 0 & f_1(z) & 0 & f_2(z) \\ 0 & 0 & 1 & 0 & 0 & 0 & 0 \end{bmatrix}. \tag{20}$$

The kinetic energy T is, therefore,

$$T = \frac{1}{2}\int_A \left(\sum_{k=1}^{nl} \int_{z_{k-1}}^{z_k} \rho^{(k)} \dot{\delta}^T [\bar{N}]^T [\bar{N}] \dot{\delta} \, \mathrm{d}z \right) \mathrm{d}A = \frac{1}{2}\int_A \dot{\delta}^T [m] \dot{\delta} \, \mathrm{d}A, \tag{21}$$

where $[m]$ is an inertia matrix, given as

$$[m] = \sum_{k=1}^{nl} \int_{z_{k-1}}^{z_k} \rho^{(k)} \dot{\varphi}^T [\bar{N}]^T [\bar{N}] \dot{\varphi} \, \mathrm{d}z = \begin{bmatrix} p & 0 & 0 & q_1 & 0 & q_2 & 0 \\ 0 & p & 0 & 0 & q_1 & 0 & q_2 \\ 0 & 0 & p & 0 & 0 & 0 & 0 \\ q_1 & 0 & 0 & I_1 & 0 & I_3 & 0 \\ 0 & q_1 & 0 & 0 & I_1 & 0 & I_3 \\ q_2 & 0 & 0 & I_3 & 0 & I_2 & 0 \\ 0 & q_2 & 0 & 0 & I_3 & 0 & I_2 \end{bmatrix}, \tag{22}$$

with

$$(p, q_1, q_2, I_1, I_2, I_3) = \left(\sum_{k=1}^{nl} \int_{z_{k-1}}^{z_k} \rho^k (1, f_1(z), f_2(2), f_1^2(z), f_2^2(z), [\, f_1(z), f_2(z)] \right) \mathrm{d}z.$$

2.2. FINITE ELEMENT MODEL

In the present work a C^0 nine-noded isoparametric quadrilateral finite element with 7 DOF per node (u, v, w, ψ_x, ψ_y, θ_x, θ_y) is employed. Initially the full plate is discretized using an eight element mesh; only the quarter plate is shown in Figure 2. Reduced integration is employed to evaluate the transverse shear

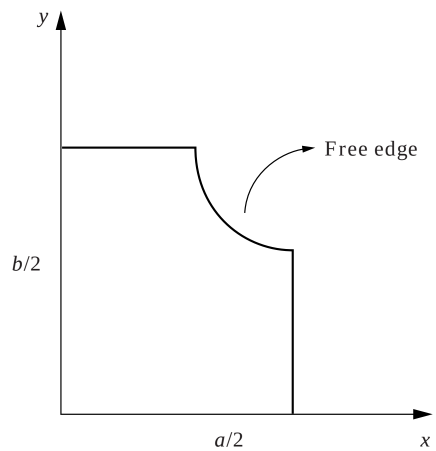

Figure 2. Quarter plate model with co-ordinates.

stresses, while full integration is used for bending and stretching. Lagrangian shape functions are used to interpolate the generalized displacements within an element. The generalized displacements within the element in terms of nodal displacements can be expressed as

$$\{\delta\}^e = \sum_{i=1}^{9}[N_i^e]\{q\}^e. \tag{23}$$

The displacement gradients can be related to the nodal displacements in the finite element modelling as

$$[d_{b_i}] = \begin{bmatrix} N_{i,x} & 0 & 0 & 0 & 0 & 0 & 0 \\ N_{i,y} & 0 & 0 & 0 & 0 & 0 & 0 \\ 0 & N_{i,x} & 0 & 0 & 0 & 0 & 0 \\ 0 & N_{i,y} & 0 & 0 & 0 & 0 & 0 \\ 0 & 0 & N_{i,x} & 0 & 0 & 0 & 0 \\ 0 & 0 & N_{i,y} & 0 & 0 & 0 & 0 \\ 0 & 0 & 0 & C_1N_{i,x} & 0 & 0 & 0 \\ 0 & 0 & 0 & 0 & C_1N_{i,y} & 0 & 0 \\ 0 & 0 & 0 & C_1N_{i,y} & C_1N_{i,x} & 0 & 0 \\ 0 & 0 & 0 & -C_2N_{i,x} & 0 & -C_4N_{i,x} & 0 \\ 0 & 0 & 0 & 0 & -C_2N_{i,y} & 0 & -C_4N_{i,y} \\ 0 & 0 & 0 & -C_2N_{i,y} & -C_2N_{i,x} & -C_4N_{i,y} & -C_4N_{i,x} \end{bmatrix}\{q\}, \tag{24}$$

or

$$[d_{MB_i}] = [B_{MB}]\{q_{MB}\}, \tag{25}$$

$$[d_{s_i}] = \begin{bmatrix} 0 & 0 & N_{i,x} & 1 & 0 & 0 & 0 \\ 0 & 0 & N_{i,y} & 0 & 1 & 0 & 0 \\ 0 & 0 & 0 & -3 & 0 & -3 & 0 \\ 0 & 0 & 0 & 0 & -3 & 0 & -3 \end{bmatrix}\{q\}, \tag{26}$$

or

$$[d_{S_i}] = [B_S]\{q_S\}. \tag{27}$$

The element stiffness matrices can now be written as

$$\begin{aligned}
[K_e] &= \int_{-1}^{1}\int_{-1}^{1} B_{MB}^T[NA]B_{MB}J\,\mathrm{d}\psi\,\mathrm{d}\eta,\\
[K_{NL1_e}] &= \int_{-1}^{1}\int_{-1}^{1} B_{MB}^T[NB]B_{MB}J\,\mathrm{d}\psi\,\mathrm{d}\eta,\\
[K_{NL2_e}] &= \int_{-1}^{1}\int_{-1}^{1} B_{MB}^T[NC]B_{MB}J\,\mathrm{d}\psi\,\mathrm{d}\eta,\\
[K_{S_e}] &= \int_{-1}^{1}\int_{-1}^{1} B_S^T[NS]B_SJ\,\mathrm{d}\psi\,\mathrm{d}\eta.
\end{aligned} \tag{28}$$

Assembling these element matrices to get global matrices and vectors, the strain energy becomes

$$U = \frac{1}{2}\int\int d^T\left[\frac{1}{2}[K_{MB}] + \frac{1}{6}[K_{NL1}] + \frac{1}{12}[K_{NL2}] + \frac{1}{2}[K_s]\right]d\,\mathrm{d}x\,\mathrm{d}y. \tag{29}$$

The Lagrangian equation of motion for free vibration is given by

$$\frac{\mathrm{d}}{\mathrm{d}t}\left(\frac{\partial T}{\partial \dot{q}_i}\right) - \frac{\partial U}{\partial q_i} = 0. \tag{30}$$

Substituting the strain energy and kinetic energy expressions into equation (30), the governing equation for the non-linear eigenvalue problem is obtained as

$$[M]\{\ddot{\delta}\} + \left[[K_{MB}] + \frac{1}{2}[K_{NL1}] + \frac{1}{3}[K_{NL2}] + [K_s]\right]\{\delta\} = 0. \tag{31}$$

Equation (31) is solved using the solution procedure for the direct iteration method suggested in references [11, 28–30].

At the point of maximum amplitude

$$\{\ddot{\delta}\} = -\omega^2\{\delta\},\ \{\dot{\delta}\} = 0.$$

Let

$$[K^L] = [K_{MB}] + [K_S], \tag{32}$$

$$[K^{NL}] = \frac{1}{2}[K_{NL1}] + \frac{1}{3}[K_{NL2}]. \tag{33}$$

The non-linear eigenvalue problem is now reduced to

$$[K^L + K^{NL}(\delta)]\{\delta\} - \omega^2[M]\{\delta\} = 0. \tag{34}$$

The solution of equation (34) is obtained using the direct iteration method. The steps involved are:

Step 1. The linear eigenvalue problem is solved by setting the amplitude to zero in equation (34).

Step 2. The mode shape of the desired non-linear mode is normalized with respect to the given amplitude at the point of maximum deflection.

Step 3. Using the normalized mode shape, the non-linear stiffness matrix $[K_{NL}]$ is computed.

Step 4. The equations are then solved to obtain new eigenvalues and corresponding eigenvectors.

Step 5. Steps (2)–(4) are repeated until convergence is attained for $\{\delta\}_{max}$ as well as ω^2 corresponding to this mode shape.

3. NUMERICAL EXAMPLES AND DISCUSSION

The following material properties are used for computation. These material properties are in the fiber direction.

Graphite/epoxy

Material-1: $E_1/E_2 = 40{\cdot}0$, $G_{12}/E_2 = G_{13}/E_2 = 0{\cdot}6$ $G_{23}/E_2 = 0{\cdot}5$, $\nu = 0{\cdot}25$, $\rho = 1500{\cdot}0$ kg/m^3.
Material-2: $E_1/E_2 = 15{\cdot}0$, $G_{12}/E_2 = G_{13}/E_2 = 0{\cdot}429$ $G_{23}/E_2 = 0{\cdot}357$, $\nu = 0{\cdot}25$, $\rho = 1389{\cdot}0$ kg/m^3.
Material-3: $E_1/E_2 = 25{\cdot}0$, $G_{12}/E_2 = 0{\cdot}2$, $G_{13}/E_2 = G_{23}/E_2 = 0{\cdot}2$, $\nu = 0{\cdot}25$, $\rho = 1500{\cdot}0$ kg/m^3.

Boron/epoxy

Material-4: $E_1/E_2 = 10{\cdot}0$, $G_{12}/E_2 = G_{13}/E_2 = 0{\cdot}3$ $G_{23}/E_2 = 0{\cdot}275$, $\nu = 0{\cdot}23$, $\rho = 2000{\cdot}0$ kg/m^3.

The boundary conditions considered for the quarter plate are shown in Figure 2. Unless otherwise explicitly stated, the laminate is simply supported on all edges.

Simply supported :

$$u_0 = w_0 = \psi_y = \theta_y = 0 \quad \text{at} \quad x = 0, \quad v_0 = \psi_x = \theta_x = 0 \quad \text{at} \quad x = a/2,$$

$$v_0 = w_0 = \psi_x = \theta_x = 0 \quad \text{at} \quad y = 0, \quad u_0 = \psi_y = \theta_y = 0 \quad \text{at} \quad y = b/2.$$

Clamped supported:

$$u_0 = v_0 = w_0 = \psi_x = \psi_y = \theta_x = \theta_y = 0 \quad \text{at} \quad x = 0 \quad \text{and} \quad y = 0,$$

$$v_0 = \psi_x = \theta_x = 0 \quad \text{at} \quad x = a/2, \quad u_0 = \psi_y = \theta_y = 0 \quad \text{at} \quad y = b/2.$$

TABLE 1

Validation results on large amplitude vibration of isotropic plate with square cutout ($A/h = 1{\cdot}0$, $\nu = 0{\cdot}3$, $a/h = 10{\cdot}0$)

	Frequency ratio					
	Present Quarter plate			Reddy [31] Quarter plate		
ca/a ratio	$a/h = 5{\cdot}0$	$a/h = 10{\cdot}0$	$a/h = 20{\cdot}0$	$a/h = 5{\cdot}0$	$a/h = 10{\cdot}0$	$a/h = 20{\cdot}0$
0·2	1·5743	1·5270	1·5135	1·5815	1·5121	1·4945
0·5	–	1·3651	1·3864	1·3653	1·3329	1·3248

–, Indicates that the iteration does not converge.

A validation study is carried out first with the proposed model for predicting the frequencies at large amplitudes. Table 1 gives the comparison of the present results using quarter plate models (see Figure 2) with the results given in reference [31] for isotropic square plates of $a/h = 10$ in the presence of square cutouts for various cutout ratios. From Table 1, it is observed that the present analysis yields results which are in close agreement with those of reference [31]. The maximum amplitude of vibration is taken as $A/h = 1{\cdot}0$. Comparisons of the present results for angle ply and cross ply thin square laminates with the results given in Reddy [31] are given in Table 2. The computed results are in good agreement with the results given in reference [31].

Initially, simply supported, isotropic, square, thick and moderately thick plates are analyzed. The effects of cutout and amplitude on frequency ratio are given in Table 3. The length and width of the cutout is taken as $ca/a = 0{\cdot}2$, $ca/cb = 2{\cdot}0$. Table 3 shows that the variation of frequency ratio with amplitude ratio shows a higher non-linearity for square cutout as compared to other cutouts. Frequency ratios obtained for thick plates are higher than those obtained for moderately thick plates for the same amplitude ratio. These effects of cutout size and edge conditions on an isotropic square plate with a square cutout of $a/h = 10$ and $ca/a = 0{\cdot}2$ are shown in Figure 3. It is observed that the

TABLE 2

Validation results on large amplitude vibration of two-layer angle ply square laminate with square cutout ($ca/a = 0{\cdot}2$, $a/h = 1000{\cdot}0$); *material: graphite/epoxy* ($E_1/E_2 = 40{\cdot}0$, $G_{12}/E_2 = G_{13}/E_2 = G_{23}/E_2 = 0{\cdot}5$, $\nu_{12} = 0{\cdot}25$)

	Frequency ratio			
	Present Quarter plate		Reddy [31] Quarter plate	
A/h ratio	[0°/90°]	[45°/−45°]	[0°/90°]	[45°/−45°]
0·2	1·0385	1·1509	1·0389	1·1636
0·4	1·1443	1·3233	1·1499	1·3471

TABLE 3

Variation of frequency ratio with amplitude ratio for simply supported square isotropic ($ca/a = 0{\cdot}2$, $ca/cb = 2{\cdot}0$)

a/h	Amplitude ratio A/h	Frequency ratio: Square cutout	Rectangular cutout	Circular cutout	Elliptical cutout
5·0	0·1	1·0075	1·0070	1·0065	1·0063
	0·2	1·0296	1·0277	1·0260	1·0251
	0·3	1·0654	1·0613	1·0577	1·0559
	0·4	1·1135	1·1063	1·1007	1·0976
	0·5	1·1723	1·1615	1·1538	1·1493
	0·6	1·2402	1·2252	1·2159	1·2097
	0·7	1·3156	1·2959	1·2856	1·2778
	0·8	1·3971	1·3750	1·3618	1·3525
	0·9	1·4830	1·4589	1·4436	1·4328
	1·0	1·5743	1·5443	1·5300	1·5179
10·0	0·1	1·0065	1·0060	1·0057	1·0055
	0·2	1·0260	1·0240	1·0229	1·0218
	0·3	1·0576	1·0534	1·0509	1·0486
	0·4	1·1005	1·0932	1·0891	1·0850
	0·5	1·1534	1·1425	1·1363	1·1303
	0·6	1·2150	1·2001	1·1918	1·1834
	0·7	1·2843	1·2650	1·2544	1·2436
	0·8	1·3600	1·3360	1·3233	1·3099
	0·9	1·4412	1·4125	1·3977	1·3815
	1·0	1·5270	1·4927	1·4767	1·4578

size of the cutout has considerable effect on the non-linearity of the response. Further, simply supported plates exhibit higher non-linearity than the plate with clamped edge conditions at all amplitudes and cutout ratios.

Table 4 shows the effect of cutout on large amplitude vibration of four-layer orthotropic laminates of $a/h = 50$, with all the edges either simply supported or clamped. It is observed from the table that the laminate with rectangular cutout results in higher non-linearity in frequency response. For the same cutout length the laminate with circular cutout results in higher frequency ratios than the square cutout for both edge conditions. The effect of cutout on large amplitude vibration for an anisotropic laminate with fibers oriented at 45° and with $a/h = 50$ is presented in Table 5. Here, the laminate with a circular cutout gives higher frequency ratios at all amplitude ratios. Further, it is observed that the laminate with a square cutout shows higher hardening effects for both orthotropic and anisotropic laminates when compared with other cutout shapes. A comparison of the circular and elliptical cutouts shows that the former gives higher hardening for both the orientations and edge conditions. This effect of increase in hardening in the presence of rectangular cutout is not observed in the case of the isotropic plate.

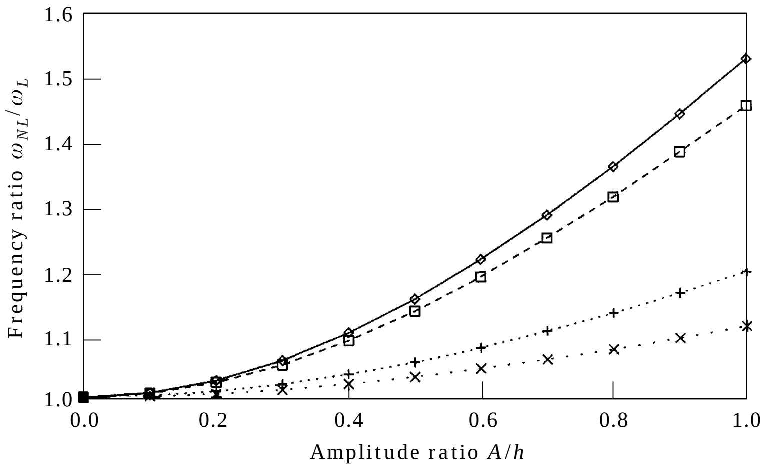

Figure 3. Effect of cutout size and edge conditions on an isotropic square plate with square cutout ($a/h = 10$, $ca/a = 0{\cdot}2$). $\diamondsuit$, $ca/a = 0{\cdot}2$, simply supported; $+$, $ca/a = 0{\cdot}2$, clamped supported; $\square$, $ca/a = 0{\cdot}4$, simply supported; $\times$, $ca/a = 0{\cdot}4$, clamped supported.

TABLE 4

Effect of cutout on large amplitude vibration of four-layer orthotropic laminate (0°) *using the quarter plate model* ($ca/a = 0{\cdot}3$, $a/h = 50{\cdot}0$, $ca/cb = 2{\cdot}0$, *material:* 2)

		Frequency ratio			
Boundary condition	Amplitude ratio	Square cutout	Rectangular cutout	Circular cutout	Elliptical cutout
Simply supported	0·1	1·0080	1·0098	1·0093	1·0091
	0·2	1·0318	1·0390	1·0366	1·0363
	0·3	1·0698	1·0864	1·0804	1·0804
	0·4	1·1201	1·1511	1·1382	1·1387
	0·5	1·1806	1·2315	1·2075	1·2105
	0·6	1·2533	1·3315	1·2860	1·2962
	0·7	1·3295	1·4360	1·3761	1·3869
	0·8	1·4109	1·5499	1·4694	1·4887
	0·9	1·4973	1·6672	1·5675	1·5978
	1·0	1·5866	1·8156	1·6683	1·6683
Clamped supported	0·1	1·0020	1·0024	1·0025	1·0026
	0·2	1·0079	1·0097	1·0102	1·0104
	0·3	1·0177	1·0217	1·0227	1·0234
	0·4	1·0331	1·0384	1·0410	1·0414
	0·5	1·0516	1·0595	1·0624	1·0642
	0·6	1·0741	1·0851	1·0856	1·0910
	0·7	1·0937	1·1151	1·1118	1·1212
	0·8	1·1176	1·1488	1·1397	1·1560
	0·9	1·1417	1·1871	1·1688	1·1924
	1·0	1·1670	1·2335	1·1998	1·2290

TABLE 5

Effect of cutout on large amplitude vibration of four-layer anisotropic laminate (45°) using the quarter plate model ($ca/a = 0{\cdot}3$, $a/h = 50{\cdot}0$, $ca/cb = 2{\cdot}0$, material: 2)

Boundary condition	Amplitude ratio	Frequency ratio: Square cutout	Rectangular cutout	Circular cutout	Elliptical cutout
Simply supported	0·1	1·0028	1·0029	1·0033	1·0033
	0·2	1·0112	1·0116	1·0134	1·0132
	0·3	1·0251	1·0260	1·0300	1·0295
	0·4	1·0444	1·0460	1·0530	1·0519
	0·5	1·0687	1·0711	1·0819	1·0802
	0·6	1·0978	1·1010	1·1163	1·1138
	0·7	1·1296	1·1340	1·1535	1·1509
	0·8	1·1664	1·1720	1·1967	1·1933
	0·9	1·2066	12136	1·2439	1·2396
	1·0	1·2499	1·2584	1·2946	1·2893
Clamped supported	0·1	1·0006	1·0005	1·0007	1·0007
	0·2	1·0023	1·0023	1·0028	1·0027
	0·3	1·0055	1·0052	1·0067	1·0061
	0·4	1·0098	1·0094	1·0120	1·0111
	0·5	1·0153	1·0147	1·0188	1·0172
	0·6	1·0220	1·0210	1·0269	1·0247
	0·7	1·0285	1·0279	1·0344	1·0327
	0·8	1·0367	1·0361	1·0443	1·0422
	0·9	1·0458	1·0449	1·0548	1·0528
	1·0	1·0552	1·0548	1·0667	1·0643

Figure 4 shows the effect of cutout shape on the frequency ratio of a two-layer simply supported antisymmetric angle ply laminate of $a/h = 50{\cdot}0$. For the same length of the cutout, the laminate with the square cutout gives the higher frequency ratio at all amplitude ratios. Figures 5 and 6 show the effects of the cutout shapes the frequency ratio for antisymmetric and symmetric laminates, respectively. From the figures, not much change is observed in the frequency ratios in the presence of circular and rectangular cutouts. For symmetric laminates the non-linearity produced is less when the amplitude is small while at higher amplitudes the non-linearity is greater. In all three cases the non-linearity introduced by the elliptical cutout is less.

The effect of size of the cutout on the frequency ratio of a five-layer antisymmetric angle ply square laminate of $a/h = 40$ for a square cutout is shown in Figure 7. From the figure it is observed that as ca/a increases up to 0·2 the frequency ratio also increases. For $ca/a > 0{\cdot}2$ the frequency ratio decreases for all amplitude ratios. Figure 8 shows the effect of cutout size on the frequency ratio for various amplitude ratios for a five-layer antisymmetric square cross ply laminate of $a/h = 40$ with a square cutout. For cross ply laminates, although the cutout ratio for maximum hardening effect is 0·2, there is not much change in

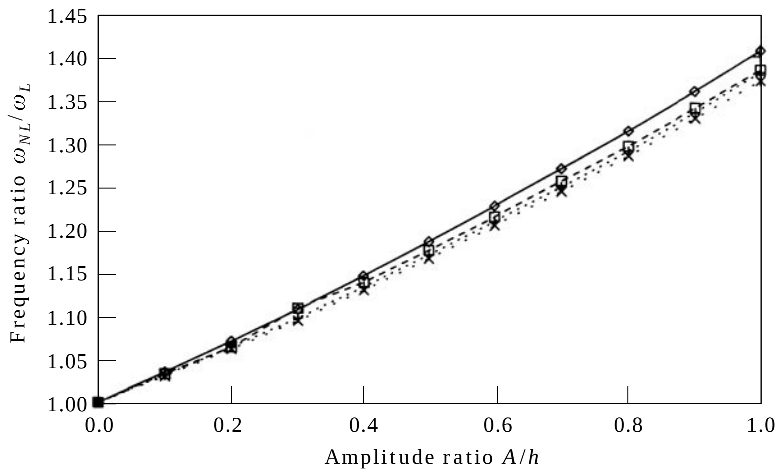

Figure 4. Variation of frequency ratio with amplitude ratio for a simply supported two-layer antisymmetric angle ply laminate in the presence of various cutout shapes ([45°/−45°] $ca/a = 0{\cdot}2$, $ca/cb = 2{\cdot}0$, $a/h = 50{\cdot}0$, material-3). ◇, Square; +, rectangular; □, circular; ×, elliptic.

the frequency ratio for $ca/a = 0{\cdot}2$ and $ca/a = 0{\cdot}3$. When the cutout ratio increases beyond 0·3 the frequency ratio decreases for all amplitude ratios. Here, the minimum hardening effect is also observed when the cutout ratio is 0·5.

Figure 9 shows the effect of cutout ratio on the frequency ratio of five-layer antisymmetric angle ply ($\theta = 45°$) square laminates of $a/h = 40$ with rectangular cutout for various amplitude ratios. When the cutout ratio is 0·2, the frequency ratio shows a maximum for all amplitude ratios. Above this value of ca/a ratio, the frequency ratio gradually decreases. The effect of cutout ratio on the

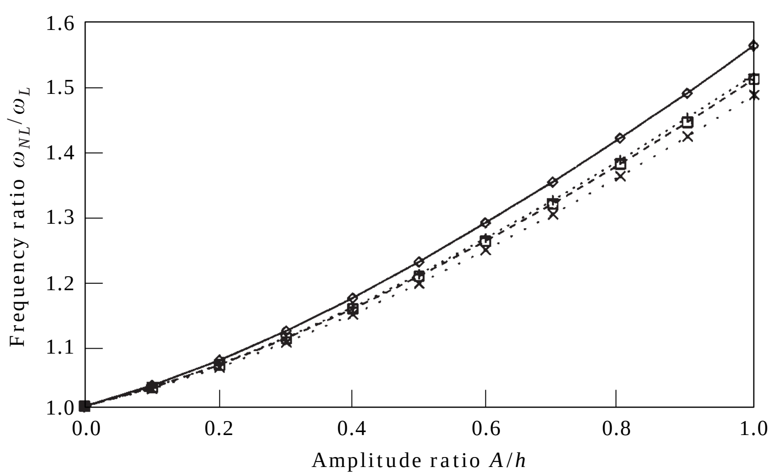

Figure 5. Variation of frequency ratio with amplitude ratio for a simply supported four-layer antisymmetric angle ply laminate in the presence of various cutout shapes ([45°/−45°/45°/−45°] $ca/a = 0{\cdot}2$, $ca/cb = 2{\cdot}0$, $a/h = 50{\cdot}0$, material-3). ◇, Square; +, rectangular; □, circular; ×, elliptic.

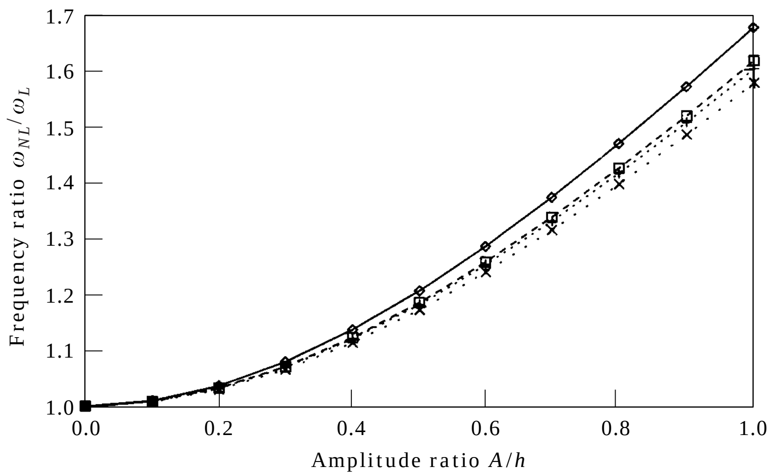

Figure 6. Variation of frequency ratio with amplitude ratio for a simply supported four-layer symmetric angle ply laminate in the presence of various cutout shapes ([45°/−45°/−45°/45°] $ca/a = 0{\cdot}2$, $ca/cb = 2{\cdot}0$, $a/h = 50{\cdot}0$, material-3). ◇, Square; +, rectangular; □, circular; ×, elliptic.

frequency ratio for five-layer antisymmetric cross ply square laminates of $a/h = 40$ for various amplitude ratios with rectangular cutout is shown in Figure 10. The frequency ratio shows a minimum value for a cutout ratio of 0·1 for all amplitude ratios. The cutout ratio corresponding to the maximum frequency ratio seems to be 0·4 for all amplitudes in the frequency ratios for the cutout ratios of 0·2, 0·3, and 0·4.

Variation of frequency ratio with amplitude ratio for a four-layer laminate in the presence of cutout with an identical area of cross-section is given in Figures 11 to 14. Figure 11 shows the variation of frequency ratio with amplitude ratio for four-layer symmetric and antisymmetric cross ply and angle ply laminates with a square cutout. It is observed that all of them produce a hardening type

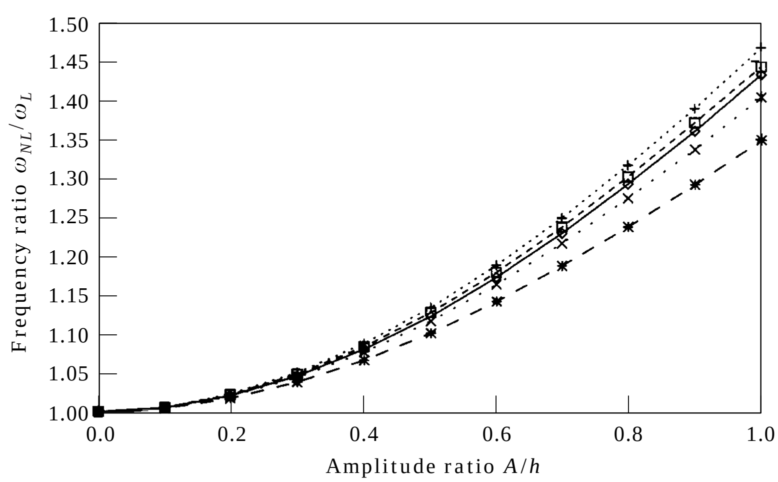

Figure 7. Effect of cutout ratio on the frequency ratio on five-layer antisymmetric angle ply square laminates of $a/h = 40$ with square cutout ([45°/−45°/45°−45°/45°], material-4). ◇, $ca/a = 0{\cdot}1$, +, $ca/a = 0{\cdot}2$; □, $ca/a = 0{\cdot}3$; ×, $ca/a = 0{\cdot}4$; *, $ca/a = 0{\cdot}5$.

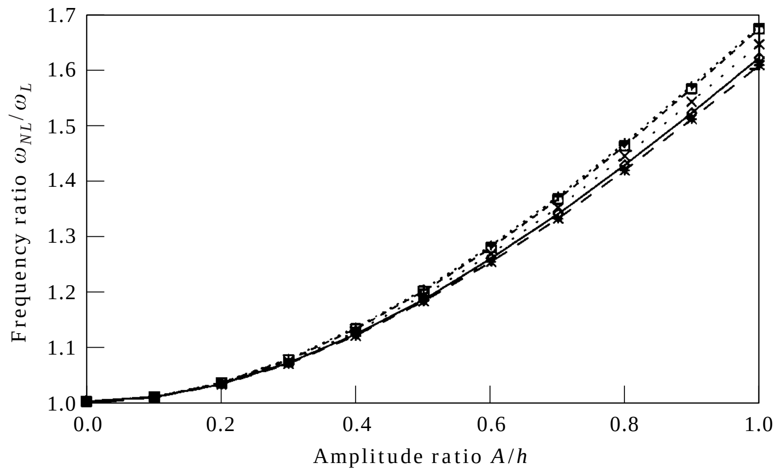

Figure 8. Effect of cutout ratio on the frequency ratio on five-layer antisymmetric cross ply square laminates of $a/h = 40$ with square cutout (material-4). ◇, $ca/a = 0{\cdot}1$, +, $ca/a = 0{\cdot}2$; □, $ca/a = 0{\cdot}3$; ×, $ca/a = 0{\cdot}4$; *, $ca/a = 0{\cdot}5$.

non-linearity. At lower amplitude ratios the antisymmetric angle ply laminate produces higher hardening effect. When the amplitude ratio increases beyond 0·6, the effect of non-linearity in the symmetric angle ply laminate is greater compared to the antisymmetric angle ply laminate.

Figure 12 shows the variation of frequency ratio with amplitude ratio for four-layer symmetric and antisymmetric, angle ply and cross ply laminates with rectangular cutout. Here, the ratio of the length of the cutout to the width of the cutout ca/cb is taken as 2·0. To keep the area of the cutout the same as the square cutout discussed above, the length of the cutout is $ca/a = 0{\cdot}56533$. As observed in the previous case on a laminate with square cutout, the

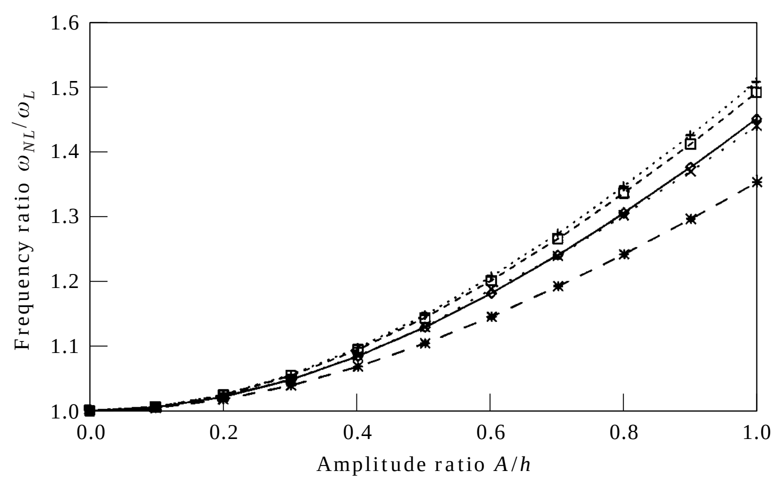

Figure 9. Effect of cutout ratio on the frequency ratio on five-layer antisymmetric angle ply square laminates of $a/h = 40$ with rectangular cutout ([45°/−45°/45°/−45°/45°], material-4). ◇, $ca/a = 0{\cdot}1$, +, $ca/a = 0{\cdot}2$; □, $ca/a = 0{\cdot}3$; ×, $ca/a = 0{\cdot}4$; *, $ca/a = 0{\cdot}5$.

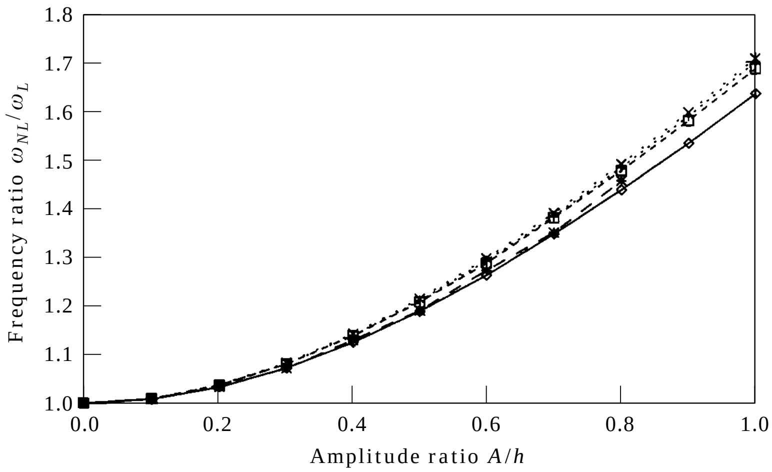

Figure 10. Effect of cutout ratio on the frequency ratio on five-layer antisymmetric cross ply square laminates of $a/h = 40$ with rectangular cutout (material-4). ◇, $ca/a = 0{\cdot}1$, +, $ca/a = 0{\cdot}2$; □, $ca/a = 0{\cdot}3$; ×, $ca/a = 0{\cdot}4$; *, $ca/a = 0{\cdot}5$.

antisymmetric angle ply laminate produces higher non-linearity than other orientations discussed here. The softening type non-linearity is observed in the case of antisymmetric cross ply laminates up to an amplitude ratio of 0·2, beyond which the hardening type of non-linearity is observed.

The effect of amplitude ratio and antisymmetric and symmetric ply orientations on the frequency ratio of a four-layer laminate with circular cutout of the same area of cross-section as discussed above is given in Figure 13. The hardening type non-linearity is observed for both symmetric and antisymmetric, cross ply and angle ply laminates. The antisymmetric cross ply laminate produces higher non-linearity at higher amplitudes. The variation of frequency

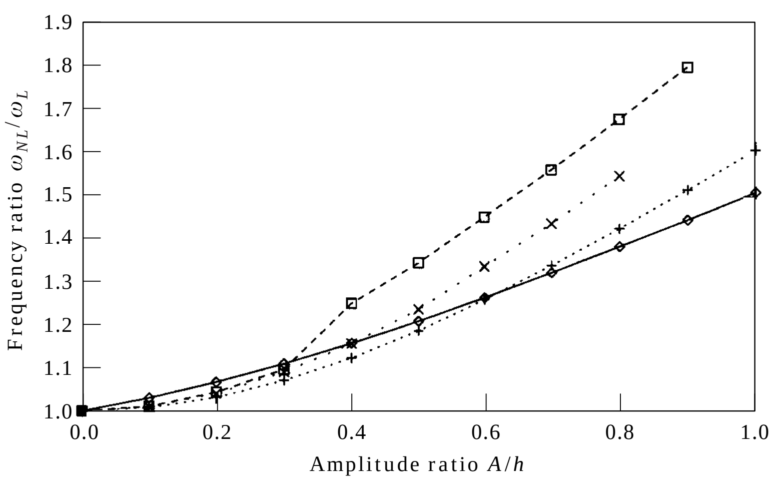

Figure 11. Variation of frequency ratio with amplitude ratio for a simply supported four-layer angle ply laminate with square cutout ($ca/a = 0{\cdot}4$, $a/h = 50{\cdot}0$, material-3). ◇, 45/−45/45/−45; +, 45/−45/−45/45; □, 0/90/0/90; ×, 0/90/90/0.

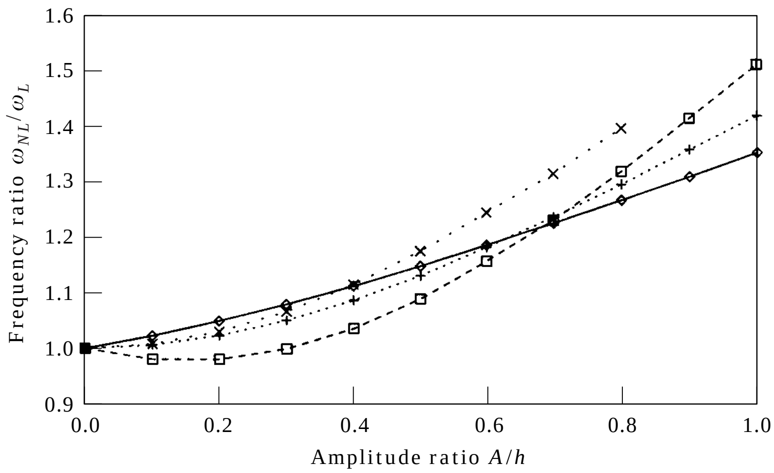

Figure 12. Variation of frequency ratio with amplitude ratio for a simply supported four-layer angle ply laminate with rectangular coutout (ca/a = 0·565333, ca/cb = 2·0, a/h = 50·0, material-3). $\diamondsuit$, 45/−45/45/−45; +, 45/−45/−45/45; $\square$, 0/90/0/90; $\times$, 0/90/90/0.

ratio with amplitude ratio for a four-layer laminate with elliptical cutout of the same area of cross-section as used in the square cutout, is given in Figure 14. Here also, a softening type non-linearity is observed for an amplitude ratio up to 0·2 for antisymmetric cross ply laminates. At higher amplitudes the symmetric cross ply laminates produce higher non-linearity than other layups. From the above figures it is observed that for the same area of cross-section, the laminate with circular cutout produces higher non-linearity than the laminate with square cutout for all layups discussed here. A softening type behavior is observed only with elliptical and rectangular cutouts.

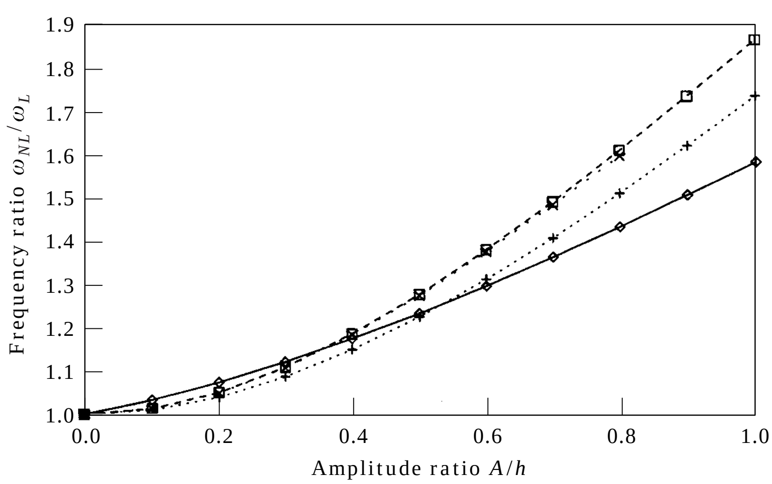

Figure 13. Variation of frequency ratio with amplitude ratio for a simply supported four-layer angle ply laminate with circular cutout (ca/a = 0·451333, a/h = 50·0, material-3). $\diamondsuit$, 45/−45/45/−45; +, 45/−45/−45/45; $\square$, 0/90/0/90; $\times$, 0/90/90/0.

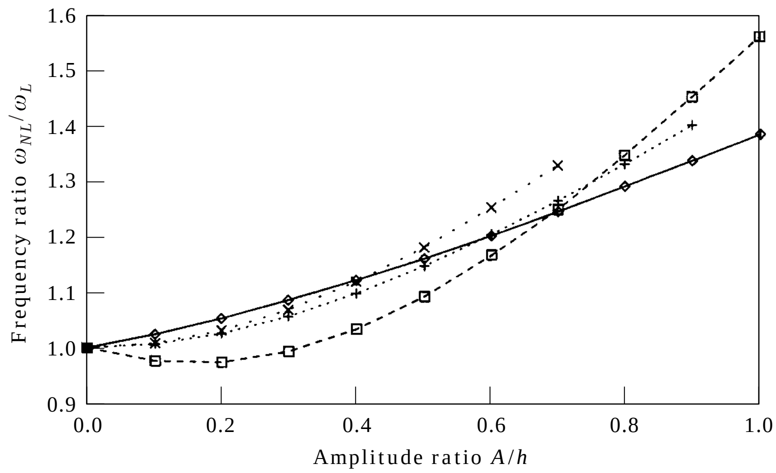

Figure 14. Variation of frequency ratio with amplitude ratio for a simply supported four-layer angle ply laminate with rectangular cutout ($ca/a = 0{\cdot}638$, $ca/cb = 2{\cdot}0$, $a/h = 50{\cdot}0$, material-3). ◇, 45/−45/45/−45; +, 45/−45/−45/45; □, 0/90/0/90; ×, 0/90/90/0.

The effect of fiber orientation on the frequency ratio of a three-layer antisymmetric angle ply laminate with rectangular cutout ($ca/a = 0{\cdot}3$, $ca/cb = 2{\cdot}0$) of $a/h = 50$ is given in Figure 15. It is interesting to note that when the 45° layer forms the outer layer (layup-1) the non-linearity produced is much higher than when it forms the inner layer (layup-2). The same trend is observed in the presence of an elliptical cutout with the same ca/a and ca/cb ratios for both the layups (see Figure 16). The response curve is identical in the case of layup-2 for both the cutout shapes while for layup-1 the laminate with rectangular cutout gives higher non-linearity. In the case of a three-layer cross ply laminate with

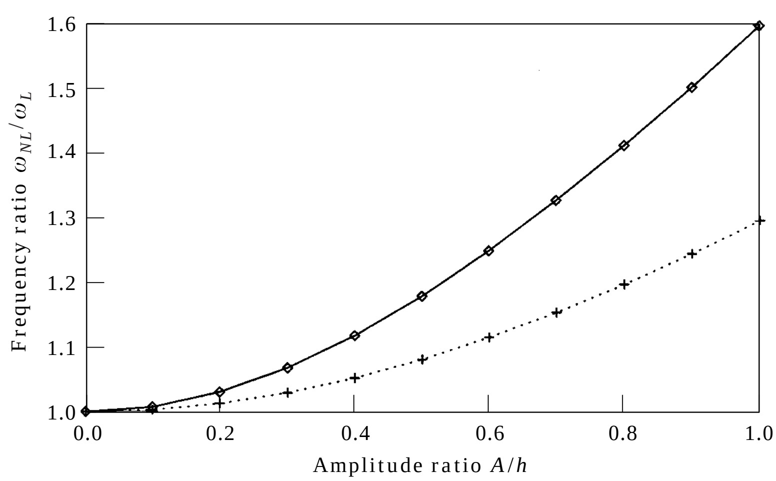

Figure 15. Effect of fiber orientation on the frequency ratio on an antisymmetric angle ply laminate with rectangular cutout for various amplitude ratios ($ca/a = 0{\cdot}2$, $ca/cb = 2{\cdot}0$, $a/h = 50{\cdot}0$, material-3). ◇, [45/−45/45]; +, [−45/45/−45].

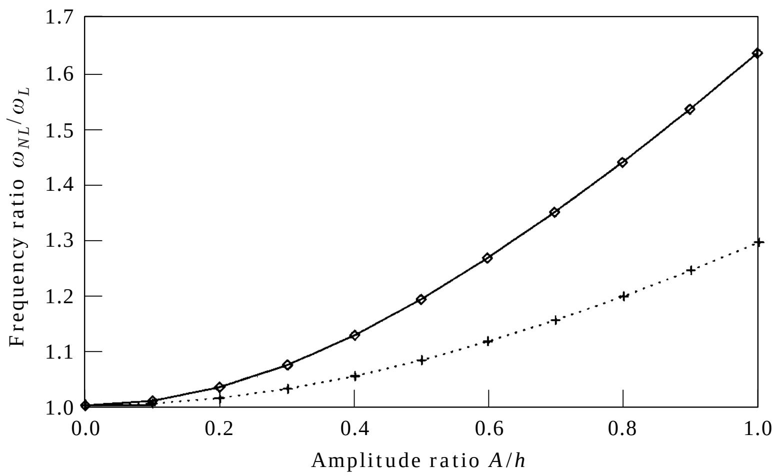

Figure 16. Effect of fiber orientation on the frequency ratio on an antisymmetric angle ply laminate with elliptic cutout for various amplitude ratios ($ca/a = 0{\cdot}2$, $ca/cb = 2{\cdot}0$, $a/h = 50{\cdot}0$, material-3). $\diamond$, [45/−45/45]; +, [−45/45/−45].

elliptical cutout shown in Figure 17, there is no change in the response whether 0° lamina forms the outer layer or inner layer.

The effects of shape and size of the cutouts on the frequency ratio for various amplitude ratios of a four-layer symmetric cross-ply laminate with clamped edges are given in Figures 18 and 19. In Figure 18 variation of frequency ratios for a cutout ratio of 0·5 is shown. It is observed from this figure that the elliptical cutout has considerable effect on the response as compared to the square cutout. However, when the cutout ratio is 0·25 (see Figure 19), the

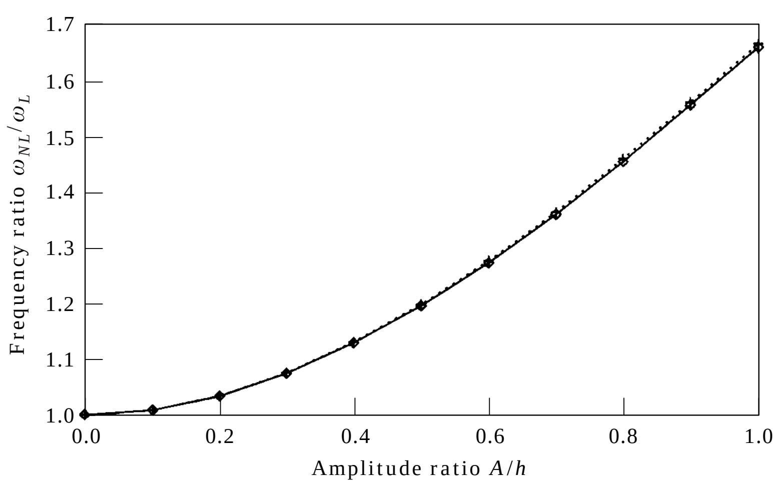

Figure 17. Effect of fiber orientation on the frequency ratio on an antisymmetric cross ply laminate with elliptic cutout for various amplitude ratios ($ca/a = 0{\cdot}2$, $ca/cb = 2{\cdot}0$, $a/h = 50{\cdot}0$, material-3). $\diamond$, [0/90/0]; +, [90/0/90].

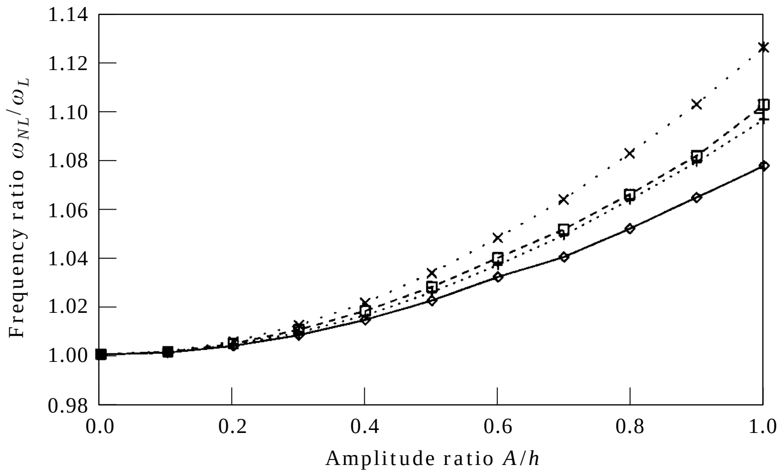

Figure 18. Effect of frequency ratio with various amplitude ratio and cutouts for a four-layer symmetric clamped square laminate ($ca/a = 0{\cdot}5$, $a/h = 500$, material-1). ◇, Square; +, rectangular; □, circular; ×, elliptical.

response is more for circular cutouts as compared to rectangular cutouts. Further, the cutout ratio has a significant effect on the response.

4. CONCLUSION

The present finite element model predicts the behavior in the large amplitude range quite satisfactorily. Presence of cutout and its shape have a significant effect on the behavior of the laminate in the large amplitude range. It is observed in general that when the cutout ratio increases up to 0·2 the non-linearity

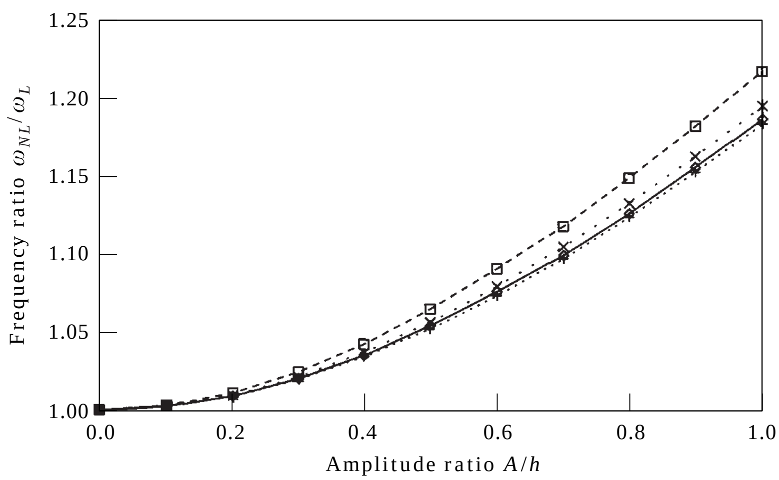

Figure 19. Effect of frequency ratio with various amplitude ratio and cutouts for a four-layer symmetric clamped square laminate ($ca/a = 0{\cdot}25$, $a/h = 500$, material-1). ◇, Square; +, rectangular; □, circular; ×, elliptical.

increases and it gradually decreases for further increase in cutout ratio. These aspects have to be kept in mind while designing composite laminated plates with cutouts. When the amplitude ratio increases beyond 0·6, the effect of non-linearity for a symmetric angle ply laminate is greater compared to the antisymmetric angle ply laminate in the presence of square cutout. It is observed that for the same cutout area the laminate with circular cutout produces higher non-linearity than the laminate with square cutout for all layups discussed above. It is also noted that the antisymmetric cross ply laminates produces a softening type of behavior in the presence of rectangular and elliptical cutouts.

REFERENCES

1. S. Woinowsky-Krieger 1950 *Transactions of ASME* **17**, 35–36. The effect of an axial force on the vibration of hinged bar.
2. T. Wah 1963 *Journal of Engineering Mechanics Division, ASCE*. **89**, 1–15. Vibrations of circular plates at large amplitudes.
3. H. N. Chu and G. Herrman 1956 *Journal of Applied Mechanics* **23**, 523–540. Influence of large amplitudes on free flexural vibrations of rectangular elastic plates.
4. N. Yamaki 1961 *Zeitschrift fur Angewandte mathematik* **41**, 501–510. Influence of large amplitudes on flexural vibrations of elastic plates.
5. B. B. Aalami 1984 *Journal of Applied Mechanics* **51**, 935–937. Large amplitude vibrations of rectangular plates.
6. C. Mei 1973 *Computers and Structures* **3**, 163–174. Finite element displacement method for large amplitude free flexural vibrations of beams and plates.
7. G. V. Rao, I. S. Raju and K. K. Raju 1976 *Computers and Structures* **6**, 163–167. A finite element formulation for large amplitude flexural vibration of rectangular plates.
8. R. Chandra and B. Basavaraju 1975 *Journal of Sound and Vibration* **40**, 393–408. Large deflection vibration of angle ply laminated plates.
9. C. Ramesh and B. Basavaraju 1975 *Fiber Science and Technology* **8**, 243–262. Large amplitude flexural vibration of cross ply laminated composite plates.
10. I. S. Raju, G. Venkateswara Rao and Kanaka Raju 1976 *Journal of Sound and Vibration* **49**, 415–422. Effect of longitudinal or inplane deformation and inertia on the larger amplitude flexural vibrations of slender beams and thin plates.
11. K. Kanaka Raju and E. Hinton 1980 *International Journal of Numerical Methods in Engineering* **16**, 247–257. Nonlinear vibrations of thick plates using mindlin plate elements.
12. J. N. Reddy and W. C. Chao 1981 *Computers and Structures* **13**, 341–347. Large-deflection and large amplitude free vibrations of laminated composite material plates.
13. J. N. Reddy 1984 *Transactions of the American Society of Mechanical Engineers*, *Journal of Applied Mechanics* **51**, 745–752. A simple higher order theory for laminated composite plates.
14. N. S. Putcha and J. N. Reddy 1986 *Computers and Structures* **22**, 529–538. A refined mixed shear flexible finite element for the nonlinear analysis of laminated plates.
15. S. Gajbir, G. Venkateswara Rao and N. G. R. Iyengar 1991 *Composite Structures* **18**, 77–91. Some observations on the large amplitude bending of rectangular antisymmetric cross-ply plates.
16. S. Gajbir, G. Venkateswara Rao and N. G. R. Iyengar 1992 *Computers and Structures* **42**, 471–480. Nonlinear bending of thin an thick unsymmetrically laminated beams using refined finite element model.

17. S. Gajbir, G. Venkateswara Rao and N. G. R. Iyengar 1993 *Composite Engineering* **3**, 507–525. Large deflection of shear deformable composite plates using a simple higher order theory.
18. S. Gajbir, G. Venkateswara Rao and N. G. R. Iyengar 1990 *Journal of Sound and Vibration* **143**, 351–355. Reinvestigation of large amplitude free vibrations of beams using finite element.
19. S. Gajbir, G. Venkateswara Rao and N. G. R. Iyengar 1991 *Journal of the American Institute of Aeronautics and Astronautics* **29**, 1727–1735. Analysis of the nonlinear vibrations of unsymmetrically laminated composite beams.
20. S. Gajbir, G. Venkateswara Rao and N. G. R. Iyengar 1990 *Journal of Sound and Vibration* **142**, 213–226. Nonlinear forced vibrations of antisymmetric rectangular cross-ply plates.
21. K. Chandrasekhara and R. Tenneti 1994 *Composite Science and Technology* **51**, 85–94. Nonlinear static and dynamic analysis of heated laminated plates: a finite element approach.
22. B. Bharat, S. Gajbir and G. Venkateswara Rao 1991 *Composite Structures* **18**, 263–282. An iteration method for the large amplitude flexural vibration of antisymmetric cross ply rectangular plates.
23. Y. Shi and C. Mei 1996 *Journal of Sound and Vibration* **193**, 453–465. A finite element time domain model formulation for large amplitude free vibrations of beams and plates.
24. Y. Shi, R. Y. Y. Lee and C. Mei 1997 *Journal of the American Institute of Aeronautics and Astronautics* **35,** 159–166. Finite element method for nonlinear free vibrations of composite plates.
25. C. A. Shankara and N. G. R. Iyengar 1996 *Journal of Sound and Vibration* **191,** 721–738. A C^0 element for the free vibration analysis of laminated composite plates.
26. C. Y. Chia 1980 *Nonlinear Analysis of Plates*. New York: McGraw-Hill.
27. S. Rajasekaran and D. W. Murrary 1973 *Journal of the Structural Engineering Division, ASCE* **99**, 2423–2438. On incremental finite element matrices.
28. M. Ganapathi and T. K. Varadan 1991 *Computers and Structures* **39**, 685–688. Nonlinear flexural vibrations of laminated orthotropic plates.
29. R. Tenneti and K. Chandrasekhara 1994 *Advances in Composite Materials* **4**, 145–158. Nonlinear vibration of laminated plates using a refined shear flexible finite element.
30. K. Decha Umphai and C. Mei 1985 *Journal of the American Institute of Aeronautics and Astronautics* **23**, 1104–1110. A finite element method for nonlinear forced vibrations of rectangular plates.
31. J. N. Reddy 1982 *Journal of Sound and Vibration* **83**, 1–10. Large amplitude flexural vibration of layered composite plates with cutouts.

Appendices overleaf

APPENDIX A

$$
[NA] = \begin{bmatrix}
A_{11} & A_{16} & A_{16} & A_{12} & 0 & 0 & B_{11} & B_{12} & B_{16} & E_{11} & E_{12} & E_{16} \\
 & A_{66} & A_{66} & A_{26} & 0 & 0 & B_{16} & B_{26} & B_{66} & E_{16} & E_{26} & E_{66} \\
 & & A_{66} & A_{26} & 0 & 0 & B_{16} & B_{26} & B_{66} & E_{16} & E_{26} & E_{66} \\
 & & & A_{22} & 0 & 0 & B_{12} & B_{22} & B_{26} & E_{12} & E_{22} & E_{26} \\
 & & & & 0 & 0 & 0 & 0 & 0 & 0 & 0 & 0 \\
 & & & & & 0 & 0 & 0 & 0 & 0 & 0 & 0 \\
 & & & & & & D_{11} & D_{12} & D_{16} & F_{11} & F_{12} & F_{16} \\
 & & & & & & & D_{22} & D_{26} & F_{21} & F_{22} & F_{26} \\
 & & & & & & & & D_{66} & F_{16} & F_{26} & F_{66} \\
 & & & & & & & & & H_{11} & H_{12} & H_{16} \\
 & & & & & & & & & & H_{22} & H_{26} \\
 & & & & & & & & & & & H_{66}
\end{bmatrix},
$$

$$
[NB_1] = \begin{bmatrix}
0 & 0 & 0 & 0 & A_{11}w_{,x} + A_{16}w_{,y} & A_{12}w_{,y} + A_{16}w_{,x} & 0 & 0 & 0 & 0 & 0 & 0 \\
 & 0 & 0 & 0 & A_{16}w_{,x} + A_{66}w_{,y} & A_{26}w_{,y} + A_{66}w_{,x} & 0 & 0 & 0 & 0 & 0 & 0 \\
 & & 0 & 0 & A_{16}w_{,x} + A_{66}w_{,y} & A_{26}w_{,y} + A_{66}w_{,x} & 0 & 0 & 0 & 0 & 0 & 0 \\
 & & & 0 & A_{12}w_{,x} + A_{26}w_{,y} & A_{22}w_{,y} + A_{26}w_{,x} & 0 & 0 & 0 & 0 & 0 & 0 \\
 & & & & \begin{array}{c} A_{11}u_{,x} + A_{12}u_{,y} \\ +A_{16}(u_{,y} + v_{,x}) \end{array} & \begin{array}{c} A_{16}u_{,x} + A_{26}v_{,y} \\ +A_{66}(u_{,y} + v_{,x}) \end{array} & 0 & 0 & 0 & 0 & 0 & 0 \\
 & & & & & \begin{array}{c} A_{12}u_{,x} + A_{26}v_{,y} \\ +A_{26}(u_{,y} + v_{,x}) \end{array} & 0 & 0 & 0 & 0 & 0 & 0 \\
 & & & & & & 0 & 0 & 0 & 0 & 0 & 0 \\
 & & & & & & & 0 & 0 & 0 & 0 & 0 \\
 & & & & & & & & 0 & 0 & 0 & 0 \\
 & & & & & & & & & 0 & 0 & 0 \\
 & & & & & & & & & & 0 & 0 \\
 & & & & & & & & & & & 0
\end{bmatrix},
$$

$$
[NB_3] = \left[\begin{array}{cccccccccccc}
0 & 0 & 0 & 0 & 0 & 0 & 0 & 0 & 0 & 0 & 0 & 0 \\
 & 0 & 0 & 0 & 0 & 0 & 0 & 0 & 0 & 0 & 0 & 0 \\
 & & 0 & 0 & 0 & 0 & 0 & 0 & 0 & 0 & 0 & 0 \\
 & & & 0 & 0 & 0 & 0 & 0 & 0 & 0 & 0 & 0 \\
 & & & & 0 & 0 & 0 & 0 & 0 & 0 & 0 & 0 \\
 & & & & \begin{array}{c} E_{11}\theta_{x,x}+ \\ E_{12}\theta_{y,y}+ \\ E_{16}(\theta_{x,y}+\theta_{y,x}) \end{array} & \begin{array}{c} E_{16}\theta_{x,x}+ \\ E_{26}\theta_{y,y}+ \\ E_{66}(\theta_{x,y}+\theta_{y,x}) \end{array} & 0 & 0 & 0 & \begin{array}{c} E_{11}w_{,x}+ \\ E_{16}w_{,y} \end{array} & \begin{array}{c} E_{12}w_{,x}+ \\ E_{26}w_{,y} \end{array} & \begin{array}{c} E_{66}w_{,y}+ \\ E_{16}w_{,x} \end{array} \\
 & & & & & \begin{array}{c} E_{22}\theta_{y,y}+ \\ E_{12}\theta_{x,x}+ \\ E_{26}(\theta_{x,y}+\theta_{y,x}) \end{array} & 0 & 0 & 0 & \begin{array}{c} E_{12}w_{,y}+ \\ E_{16}w_{,x}+ \end{array} & \begin{array}{c} E_{22}w_{,y}+ \\ E_{26}w_{,x}+ \end{array} & \begin{array}{c} E_{66}w_{,x}+ \\ E_{26}w_{,y}+ \end{array} \\
 & & & & & & 0 & 0 & 0 & 0 & 0 & 0 \\
 & & & & & & & 0 & 0 & 0 & 0 & 0 \\
 & & & & & & & & 0 & 0 & 0 & 0 \\
 & & & & & & & & & 0 & 0 & 0 \\
 & & & & & & & & & & 0 & 0 \\
 & & & & & & & & & & & 0
\end{array}\right],
$$

$$
[NB_2] = \begin{bmatrix}
0 & 0 & 0 & 0 & 0 & 0 & 0 & 0 & 0 & 0 & 0 & 0 \\
 & 0 & 0 & 0 & 0 & 0 & 0 & 0 & 0 & 0 & 0 & 0 \\
 & & 0 & 0 & 0 & 0 & 0 & 0 & 0 & 0 & 0 & 0 \\
 & & & 0 & 0 & 0 & 0 & 0 & 0 & 0 & 0 & 0 \\
 & & & & \begin{matrix} B_{11}\theta_{x,x}+ \\ B_{12}\theta_{y,y}+ \\ B_{16}(\theta_{x,y}+\theta_{y,x}) \end{matrix} & \begin{matrix} B_{16}\theta_{x,x}+ \\ B_{26}\theta_{y,y}+ \\ B_{66}(\theta_{x,y}+\theta_{y,x}) \end{matrix} & \begin{matrix} B_{11}w_{,x}+ \\ B_{16}w_{,y} \end{matrix} & \begin{matrix} B_{12}w_{,x}+ \\ B_{26}w_{,y} \end{matrix} & \begin{matrix} B_{66}w_{,y}+ \\ B_{16}w_{,x} \end{matrix} & \begin{matrix} E_{11}w_{,x}+ \\ E_{16}w_{,y}+ \end{matrix} & \begin{matrix} E_{12}w_{,x}+ \\ E_{26}w_{,y}+ \end{matrix} & \begin{matrix} E_{66}w_{,y}+ \\ E_{16}w_{,x} \end{matrix} \\
 & & & & & \begin{matrix} B_{22}\theta_{y,y}+ \\ B_{12}\theta_{x,x}+ \\ B_{26}(\theta_{x,y}+\theta_{y,x}) \end{matrix} & \begin{matrix} B_{12}w_{,y}+ \\ B_{16}w_{,x} \end{matrix} & \begin{matrix} B_{22}w_{,y}+ \\ B_{26}w_{,x} \end{matrix} & \begin{matrix} B_{66}w_{,x}+ \\ B_{26}w_{,y} \end{matrix} & \begin{matrix} E_{12}w_{,y}+ \\ E_{16}w_{,x} \end{matrix} & \begin{matrix} E_{22}w_{,y}+ \\ E_{26}w_{,x} \end{matrix} & \begin{matrix} E_{66}w_{,x}+ \\ E_{26}w_{,y} \end{matrix} \\
 & & & & & & 0 & 0 & 0 & 0 & 0 & 0 \\
 & & & & & & & 0 & 0 & 0 & 0 & 0 \\
 & & & & & & & & 0 & 0 & 0 & 0 \\
 & & & & & & & & & 0 & 0 & 0 \\
 & & & & & & & & & & 0 & 0 \\
 & & & & & & & & & & & 0
\end{bmatrix},
$$

$$[NC] = \begin{bmatrix} 0 & 0 & 0 & 0 & 0 & 0 & 0 & 0 & 0 & 0 & 0 & 0 \\ & 0 & 0 & 0 & 0 & 0 & 0 & 0 & 0 & 0 & 0 & 0 \\ & & 0 & 0 & 0 & 0 & 0 & 0 & 0 & 0 & 0 & 0 \\ & & & 0 & 0 & 0 & 0 & 0 & 0 & 0 & 0 & 0 \\ & & & & A & B & 0 & 0 & 0 & 0 & 0 & 0 \\ & & & & & C & 0 & 0 & 0 & 0 & 0 & 0 \\ & & & & & & 0 & 0 & 0 & 0 & 0 & 0 \\ & & & & & & & 0 & 0 & 0 & 0 & 0 \\ & & & & & & & & 0 & 0 & 0 & 0 \\ & & & & & & & & & 0 & 0 & 0 \\ & & & & & & & & & & 0 & 0 \\ & & & & & & & & & & & 0 \end{bmatrix},$$

where

$$A = \frac{3}{2}A_{11}w_{,x}^2 + 3A_{16}w_{,x}w_{,y} + A_{66}w_{,y}^2,$$

$$B = A_{12}w_{,x}w_{,y} + \frac{3}{2}A_{16}w_{,x}^2 + \frac{3}{2}A_{26}w_{,y}^2 + 2A_{66}w_{,x}w_{,y},$$

$$C = \frac{3}{2}A_{22}w_{,y}^2 + 3A_{26}w_{,x}w_{,y} + \frac{1}{2}A_{12}w_{,x}^2 + A_{66}w_{,y}^2.$$

APPENDIX B: NOTATION

a, b	length and width of the plate
ca, cb	length and width of the cutout
A/h	amplitude ratio
$\{\varepsilon\}^L$	linear strain vector
$\{\varepsilon\}^{NL}$	non-linear strain vector
ε_p, ε_b, ε_s	membrane, bending and shear strains
ε^*, ε_s^*	higher order bending and shear strains
$[NA]$	linear stiffness matrix
$[NB]$, $[NC]$	non-linear stiffness matrices
$[NS]$	linear stiffness matrix (shear)
U_{MB}	membrane and bending strain energy
U_S	shear strain energy
$[d]$	Displacement gradient vector
$[d_s]$	Displacement gradient vector corresponding to shear terms
$\{\delta\}$	generalized displacement vector
$\{q\}$	nodal displacement vector
NL	non-linear
e	subscript for the element
ω	natural frequency
ω_{1NL}	fundamental non-linear frequency

T	kinetic energy
$[M]$	mass matrix
$[K]^L$	linear stiffness matrix
$[K]^{NL}$	non-linear stiffness matrix
W	weight of the plate
mc	material code
P_c	probability of crossover
P_m	probability of mutation